Combustion and Flame 235 (2022) 111693

Contents lists available at ScienceDirect

Combustion and Flame

journal homepage: www.elsevier.com/locate/combustflame

Numerical investigation and assessment of flamelet-based models for the prediction of pulverized solid fuel homogeneous ignition and combustion

Pooria Farmand[a,*], Hendrik Nicolai[b,c], Christoph Schumann[a], Antonio Attili[d], Lukas Berger[a], Tao Li[e], Christopher Geschwindner[e], Francesca di Mare[c], Christian Hasse[f], Benjamin Böhm[e], Johannes Janicka[b], Heinz Pitsch[a]

[a] RWTH Aachen University, Faculty of Mechanical Engineering, Institute for Combustion Technology, Templergraben 64, Aachen 52056, Germany
[b] Technical University of Darmstadt, Department of Mechanical Engineering, Energy- and Power Plant Technology, Otto-Berndt-Straße 3, Darmstadt 64287, Germany
[c] Ruhr University Bochum, Chair of Thermal Turbomachines and Aeroengines, Universitätsstraße 150, Bochum 44801, Germany
[d] University of Edinburgh, School of Engineering, Institute of Multiscale Thermofluids, The King's Buildings, Mayfield Road, Edinburgh, EH9 3FD, United Kingdom
[e] Technical University of Darmstadt, Department of Mechanical Engineering, Reactive Flows and Diagnostics, Otto-Berndt-Straße 3, Darmstadt 64287, Germany
[f] Technical University of Darmstadt, Department of Mechanical Engineering, Simulation of reactive Thermo-Fluid Systems, Otto-Berndt-Straße 2, Darmstadt 64287, Germany

ARTICLE INFO

Article history:
Received 29 October 2020
Revised 11 August 2021
Accepted 11 August 2021
Available online 30 August 2021

Keywords:
Pulverized solid fuel combustion
Particle group combustion
Homogeneous ignition
Devolatilization modeling
Detailed kinetics
FGM tabulated chemistry

ABSTRACT

The homogeneous ignition and volatile combustion of pulverized solid fuel in single-particle and particle group configurations were studied numerically in a laminar flat flame burner. Simulations with increasing particle streams were performed to investigate the influence of the interactions in particle groups on homogeneous ignition and combustion. An extensive set of simulations are conducted considering models with different levels of detail for both the gas-phase and solid fuel chemistry. The reference simulations employ the chemical percolation devolatilization model coupled with a detailed chemistry model for gas-phase reactions. The particle-fluid interactions were modeled with a fully coupled Eulerian-Lagrangian framework. Increased ignition delay times for higher particle streams were successfully validated against available experimental measurements. Furthermore, the transition from single-particle ignition to a conically shaped volatile flame with suppressed reactions near the flame base in particle group combustion was observed in both experiments and simulations. The subsequent detailed investigations revealed that the increased heat transfer to particles and, therefore, lower gas temperature for higher particle number densities together with the local oxygen depletion are the primary reasons for this transition. Based on the reference simulation, different simplified model combinations were assessed. The systematic model reduction investigation started with assessing the fixed volatile composition as a required assumption for flamelet models. Finally, the effects of gas-phase chemistry and different simple devolatilization models on ignition and combustion chemistry were studied. Overall, all model combinations provide reasonable predictions of volatile combustion with minor local deficits in the studied conditions.

1. Introduction

The accurate prediction of pulverized coal combustion (PCC) is still a significant challenge, as complex sub-processes coincide on vastly different length and time scales. In addition to the actual coal conversion, which is characterized by devolatilization and char oxidation, the mixing and particle movement in the turbulent flow, as well as the turbulence-chemistry interaction, must be considered. The increase in computational resources in recent years has improved the accuracy of computational fluid dynamics (CFD) simulations by using scale-resolving techniques [1,2]. For instance, the direct computation of essential physical sub-processes in academic cases and small-scale experiments became feasible. On the contrary, this remains prohibitive in large-scale applications

* Corresponding author.
E-mail address: p.farmand@itv.rwth-aachen.de (P. Farmand).

https://doi.org/10.1016/j.combustflame.2021.111693
0010-2180/

Nomenclature

Symbol	*Description*	*Unit*
α	Splitting ratio	-
Δx	Relative height	(mm)
$\dot{\Psi}_{\text{prt}}$	Interphase energy exchange	(J/m^{3}s)
$\dot{m}_{\text{dev}}$	Devolatilization mass release rate	(kg/s)
$\dot{N}_{\text{inj}}$	Particle injection rate	(prt/ms)
$\dot{q}_{\text{prt,dev}}$	Devolatilization energy exchange	(J/m^{3}s)
$\dot{S}_{\Phi}$	Euler source term of arbitrary quantity Φ	-
ϵ	Emissivity	-
λ	Thermal conductivity	(W/m K)
$\dot{\text{Q}}$	Heat release rate	(J/m^3 s)
m	Mass	(kg)
T	Temperature	(K)
Ω_{g}	Computational cell volume	(m^3)
ω_i	Production rate of species i	(kg/m^2 s)
ϕ^k	Gaussian distribution coefficient for particle k	-
ρ	Density	(kg/m^3)
σ	Stefan-Boltzmann constant	(W/m^{2}K^4)
τ_{ign}	ignition delay time	(ms)
c_p	Specific heat capacity at constant pressure	(J/kg s)
d	Diameter	(m)
dx	Computational cell size	(m)
e_{ign}	Relative ignition prediction error	%
h_i	Specific enthalpy of species i	(J/kg)
k_{dev}	Devolatilization rate	(1/s)
Nu	Nusselt number	-
Pr	Prandtl number	-
R	Universal gas constant	(J/kg mol)
Re	Reynolds number	-
t	Time	(ms)
U_β	Velocity in direction β	(m/s)
$V_{\beta,i}$	Diffusion velocity in β direction	(m/s)
$Y_{\text{Vol},0}$	Initial volatile fraction	-
Y_i	Mass fraction of species i	-
Z	Mixture fraction	-
A	Pre-exponential factor	(1/s)
E	Activation energy	(J/mol)

Abbreviations	*Description*
C2SM	Competing two-step model
CFD	Computational fluid dynamics
CPD	Chemical percolation devolatilization model
DBI	Diffuse backlight-illumination
FC	Finite chemistry
FF	Flat flame
FFB	Flat flame burner
FGM	Flamelet generated manifold
FVC	Fixed volatile composition
ILU	Incomplete LU-decomposition
LES	Large eddy simulation
OH-LIF	Laser-induced fluorescence of the OH radical
PCC	Pulverized coal combustion
PND	Particle number density
SFOR	Single first-order reaction model
SSS	Statistically steady-state
TVD	Total variation diminishing

Subscript	*Description*
$\cdot_{\text{g}}$	Property of gas
$\cdot_{\text{prt}}$	Property of particle
$\cdot_{\text{Vol}}$	Volatile
$\cdot_{\text{wall}}$	Wall property

in the foreseeable future. Hence, accurate PCC modeling is still required and one main focus regarding modeling efforts is the devolatilization process due to its significant impact on ignition and flame stabilization [3].

In the literature, the modeling of devolatilization and homogeneous ignition is addressed at various levels of detail. On the one hand, very detailed models such as the chemical percolation devolatilization (CPD) model, which is based on a detailed description of the molecular structure of the reference coal, are used to describe devolatilization [4]. Based on this detailed description, the model determines rates for each species released during the devolatilization process. However, these detailed models demand high computational effort, which prevents a direct coupling of such models in the simulation of large-scale applications. On the other hand, simpler one-step and two-step models are less complex alternatives to include the devolatilization kinetics by simple Arrhenius expressions in CFD simulations [5,6]. Yet, experiments or detailed models are required to determine model coefficients of the specific coal and operating conditions as well as the appropriate composition of the released volatiles [7].

Similar to solid fuel conversion, gas-phase chemistry can be described at various levels of detail, too. Here, finite-rate chemistry coupled with detailed kinetic mechanisms constitutes the most accurate but cost-intensive way to include gas-phase reactions in simulations. Alternatives to the direct use of finite-rate chemistry are flamelet-based models, which allow a very efficient representation of the detailed gas-phase kinetics in CFD simulations [8–11]. Precalculating and storing one-dimensional flamelets based on reduced variables (e.g., mixture fraction and progress variable) in a flamelet table, which is accessed during the simulation to obtain the thermo-chemical state, reduce simulation costs significantly. However, two assumptions are commonly applied for simplifying the application of flamelet-based models for PCC: First, the assumption that the composition of the complex mixture of volatiles released during devolatilization is fixed for the flamelet simulations prevents the use of additional flamelet dimensions [12]. Second, assuming that the flamelet configuration is either premixed or non-premixed eliminates the need for formulations for partially-premixed combustion, such as for instance the model by Knudsen et al. [13,14]. However, similar to the finding for spray combustion [15], investigations demonstrated the occurrence of both regimes in PCC [16]. Therefore, flamelet-based model approaches based on both non-premixed flames [8,9] and premixed flames [10,11] have been developed for also PCC.

The coupling and interaction of devolatilization and gas-phase homogeneous ignition modeling are often validated in laminar single-particle configurations. This configuration reduces the complexity of the industrial-scale system significantly by removing the influence of turbulence. Hence, the direct application of detailed numerical models and precise non-intrusive measurements due to optical accessibility are becoming possible in such configurations. Two extensively utilized configurations from the literature are the Hencken type burner from Molina and Shaddix [17,18] and the flat flame burner investigated by Köser et al. [19,20]. The first configuration was previously used to validate detailed simulations performed by Farazi et al. [21], Goshayeshi and Sutherland [22], as well as Jiménez and Gonzalo-Tirado [23], where the CPD model was directly coupled to finite-rate chemistry adopting the GRI3.0 kinetic mechanism [24] to study single-particle homogeneous ignition. All studies report an acceptable agreement in terms of ignition delay. Similar to the studies mentioned above, Vascellari et al. [8] used this configuration to validate their finite-rate chemistry simulation. Additionally, they extracted the full thermo-chemical state, which is not available from experiments, and assessed the steady-flamelet model's applicability to capture single-particle homogeneous ignition. Here, a simplified two-step

model was chosen to describe devolatilization, with the kinetic parameters being fitted using CPD calculations. Additionally, Knappstein et al. [25] used the flat flame burner reported by Köser et al. [19,20] to study a flamelet generated manifold (FGM) model for single-particle combustion and found good agreement with the ignition delay measured by laser-induced fluorescence of the OH radical (OH-LIF). In this study, a simplified one-step model with parameters determined from a drop tube reactor was used for devolatilization. Recently, Attili et al. [26] used detailed simulations employing the CPD model coupled with finite-rate chemistry to study the effect of slip velocity on single-particle homogeneous ignition and combustion in the flat flame burner of Köser et al. [19,20].

However, considering systems on a larger scale, particle group combustion gains crucial importance. Therefore, the accurate prediction of the transition from single to group particle combustion must be an essential feature of PCC models. To provide the necessary validation basis, the two experimental setups mentioned above were recently extended to investigate particle group combustion [27,28]. Both studies report a significant increase in ignition delay time at higher particle loads. Furthermore, Li et al. [28] found a transition from spherical flames around single particles to a conical flame around particle groups. This transition has been reproduced by Nicolai et al. [11] in a simulation using a competing two-step model coupled with an FGM approach. In addition, purely numerical studies also investigated the influence of the particle number density on the combustion [29–31]. Farazi et al. [29] investigated particle groups in a channel configuration and found a significantly increased ignition delay for high particle number densities. Tufano et al. [30] simulated a static arrangement of particles and found strong influences of the particle Reynolds number and particle spacing on the volatile combustion regime. While the aforementioned studies focused exclusively on volatile combustion, Sayadi et al. [31] investigated the influence of various parameters (e.g., particle spacing, oxygen concentration, particle Reynolds number, and particle arrangement) on char conversion.

While all of the aforementioned studies focus on homogeneous ignition, a competition between heterogeneous and homogeneous ignition modes can exist in PCC [32,33]. In a series of investigations, especially for small particles, the occurrence of heterogeneous ignition was observed experimentally [34]. Especially lignites, due to their high probability to undergo fragmentation, tend to ignite heterogeneously. Contrary, bituminous coals, on which most previous modeling studies focus, were found to ignite in homogeneous mode [17,35–37].

From the previous discussion, two missing modeling aspects can be identified with respect to the modeling of homogeneous ignition, which shall be tackled in this work. First, validations of detailed gas and solid kinetic models in particle group combustion are missing. Second, the evaluation of assumptions made for flamelet models is missing for such configurations. To contribute to these missing points, this work's objective is divided into three parts: (1) The detailed model for both gas phase and solid phase, necessary to accurately capture homogeneous ignition, is applied in a flat flame burner (FFB) and fully validated against available measurements. (2) The validated detailed simulation allows an in-depth analysis of the physical processes occurring during the transition from single to particle group combustion. In addition, the complete thermo-chemical state can be extracted from the detailed simulations, which allows (3) a detailed assessment of the reduced models for particle group combustion. This analysis is carried out in gradual evaluations of each individual assumption (e.g., fixed volatile composition, gas-phase, and devolatilization modeling) that are necessary for efficient solid fuel modeling. Since in this study, the main goal is to investigate the homogeneous modes in ignition and combustion of pulverized solid fuels as a part of the holistic coal model assessment, the studied conditions are chosen such that group particle combustion is pronounced and only homogeneous modes are observed for the investigated pulverized solid fuel. Hence, this study is to be understood as a detailed sub-model investigation assessing homogeneous ignition and combustion modeling for holistic coal modeling. To the best of the authors' knowledge, this study presents the first comprehensive analysis of the reduction for both gas-phase and solid-fuel kinetics in single-particle and particle group homogeneous ignition and combustion.

The remainder of the paper is structured as follows: Section 2 describes the numerical codes and models used in this paper. Section 3 briefly summarizes the experimental configuration and the measurement techniques employed. Moreover, the boundary conditions for the numerical setup are given. Section 4 presents the results, whereby first the detailed simulation results are validated against measurements. Then, the physico-chemical effect of particle group combustion at different coal mass flow rates is analyzed. This is followed by a step-by-step reduction of the overall model up to the flamelet model with simple solid fuel kinetics. Finally, the most important outcomes of this work are summarized in Section 5.

2. Numerical framework and modelling

During coal combustion, mass, momentum, and energy transfer occur between particles and the gas phase, which are modeled by an Eulerian-Lagrangian approach in this study. A two-way coupling ensures each quantities' conservation between Lagrangian and Eulerian frameworks. Throughout the study, the solver CIAO, which calculates chemical reactions by finite-rate chemistry, and the solver FASTEST, which relies on a flamelet-based description of chemical reactions, are employed. For the Lagrange phase, both codes rely on identical models, detailed below. In the following, the respective numerical frameworks are briefly outlined.

In the CIAO code, the Eulerian governing equations are solved using a semi-implicit finite difference code with second-order accuracy in space and time [21,38–40]. The low Mach number Navier–Stokes equations are solved together with the Poisson equation to satisfy continuity. The pressure solver is based on the multi-grid solver of HYPRE [41]. The Crank-Nicolson method is applied for time advancement along with an iterative predictor-corrector scheme [21,29,42]. For updating the particle state, position and the source terms for the gas phase equations, the particle equations are advanced in a Lagrangian framework using a two-stage Runge-Kutta solver with second-order accuracy. For specific information about the numerical implementation, the reader is referred to previous studies [21,29].

FASTEST is a 3D finite-volume code that uses block-structured, boundary-fitted meshes with hexahedral cells to represent complex geometries. Spatial discretization of the velocity is based on a multi-dimensional Taylor-series expansion with second-order accuracy [43]. To achieve boundedness of the scalars, a TVD limiter suggested by Zhou et al. [44] is used. The time advancement of transported quantities is computed using an explicit, three-stage Runge–Kutta scheme of second-order accuracy. The low Mach number, variable density Navier-Stokes equations are solved, where continuity is satisfied by solving a pressure correction equation within each Runge–Kutta stage. The solver is based on ILU matrix decomposition and uses the strongly implicit procedure proposed

by Stone [45]. For detailed information about the numerical implementation, the reader is referred to previous studies [11,25].

2.1. Particle modeling

Particle dynamics are modeled in a Lagrangian framework using the point-particle assumption solving equations for trajectory, velocity, mass, and temperature as described by Farazi et al. [21]. Additionally, various submodels are required to capture the full conversion process of the coal particles. Generally, devolatilization and char conversion, which occur under significantly different timescales, characterize the solid fuel conversion process. Due to substantially slower time scales, the influence of char conversion on homogeneous ignition is assumed to be negligible during devolatilization, which is in accordance with previous studies [21,25,46]. Additionally, simulations employing a state-of-the-art char conversion model [47,48] were carried out to prove the negligible effect of heterogeneous reactions on the ignition process in the current setup.

2.1.1. Devolatilization models

During devolatilization, particles undergo a strong heat-up leading to the release of gaseous matter. For the particle, the diameter d_{prt} is assumed constant during this process, while the initial particle density $\rho_{\mathrm{prt},0} = 1200\ \frac{\mathrm{kg}}{\mathrm{m}^3}$ is reduced to satisfy mass continuity [22,46]. This assumption also corresponds to the small measured geometry changes in the chosen diameter range for the selected coal in the studied configuration. Also, a previous study on a similar configuration by Attili et al. [26] has shown that the impact of a varying particle diameter on the ignition delay time is negligible justifying the constant diameter assumption. In this study, devolatilization models with varying levels of detail (from detailed phenomenological network models to simple global models) are considered, which are described below.

The chemical percolation devolatilization (CPD) model is the most accurate model considered in this study to compute the devolatilization rates. The mass rate of change $\dot{m}_{\mathrm{dev}}$ is calculated based on a detailed description of the molecular structure for the reference coal [4,49,50]. The coal lattice contains aromatic rings connected by stable and labile bridges. Stable bridges mainly appear within the infinite fragments of aromatic rings, which are referred to as char. The labile bridges can break due to the external energy in the devolatilization phase, resulting in the release of light gases and finite fragments. Finite fragments with lower molecular weight are vaporized as tar, and the heavier ones remain in the lattice and form metaplast, which can convert to char by cross-linking. Based on the chemical reaction pathway of the bridge breaking mechanism in the CPD model, the devolatilization process starts by breaking a labile bridge into a highly reactive intermediate bridge, which can then break and form light gases and tar species. The CPD model computes the formation rate and composition of the tar, light gases, and the remaining char. Then, the devolatilization rate can be computed by summing up the formation rates of tar and light gases. In the CPD model, the particle heating rate can change during the devolatilization process due to the change in particle temperature [51], leading to dynamic composition or time dependent volatile release due to the change in particle heating rate. In the present study, light gases consist of CH_4, CO_2, CO, H_2O, and other gases, which are assumed to be C_2H_2 similar to the assumption by Jimenez and Gonzalo-Tirado [23]. The rate of tar release, which is also computed by the CPD model, is assumed to be only for C_2H_2. This assumption was also used by Goshayeshi and Sutherland [22], Tufano et al. [46], and Farazi et al. [21,29]. To assess the effect of tar composition choice on the ignition delay time, other species like C_6H_6 were used as tar by Farazi et al. [21], and only a marginal difference (<3%) in ignition delay time has been observed. Although the ignition delay time of C_2H_2 in a purely gas-phase setting is much lower than that of C_6H_6 because of the different heating values, the marginal difference in t_{ign} for the particle setting shows that ignition time is dominated by the time required for particle heating.

One global model often applied in large-scale LES, is the competing two-step model (C2SM) proposed by Kobayashi et al. [6]. Here, the heating rate dependency of devolatilization is included in the model by describing mass loss using two Arrhenius type equations, for low and high heating rates, respectively. The released volatile mass $\dot{m}_{\mathrm{dev}}$ is computed according to

$$\dot{m}_{\mathrm{dev}} = k_{\mathrm{dev}}\left(m_{\mathrm{Vol},0} - m_{\mathrm{Vol}}\right) \tag{1}$$

with

$$k_{\mathrm{dev}} = \alpha_1 A_1 \mathrm{e}^{\frac{-E_1}{RT_{\mathrm{prt}}}} + \alpha_2 A_2 \mathrm{e}^{\frac{-E_2}{RT_{\mathrm{prt}}}}. \tag{2}$$

Herein, $m_{\mathrm{Vol},0}$ and m_{Vol} are the initial and current volatile mass, respectively. The initial volatile $m_{\mathrm{Vol},0}$ is calculated based on a detailed CPD simulation for a heating rate equal to the single-particle case as $m_{\mathrm{Vol},0} = m_0 Y_{\mathrm{Vol},0}$, where $Y_{\mathrm{Vol},0} = 0.5494$ denotes the initial fraction of volatiles in the particle. Comparing this value to the value of the proximate analysis presented in Table 3, a Q-factor that gives the ratio of actual volatile mass compared to the volatile mass determined by the Proximate analysis, of 1.53 can be calculated. As $m_{\mathrm{Vol},0}$ is fixed during the simulation, any Q-factor variations are not considered. Two facts can justify this assumption: First, the heating rate, which potentially changes the Q-factor, changes only slightly for the investigated operating conditions. Second, the main focus of this study is the ignition and early phase of volatile combustion. Therefore, $m_{\mathrm{Vol},0}$, which determines overall mass released, will likely not affect simulation results. The coal-specific parameters (e.g., pre-exponential constants A_1 and A_2, activation energies E_1 and E_2, and the splitting ratios α_1 and α_2) have been determined prior to this study with a method detailed in [8] and are summarized in Table 1.

One of the simplest, but still widely used models, is the single first-order reaction model (SFOR) proposed by Badzioch and Hawksley [5]. This model uses the same Eq. (1) as the C2SM model to calculate the released volatile mass $\dot{m}_{\mathrm{dev}}$. However, as the name implies, the devolatilization rate is calculated from a single Arrhenius-type equation

$$k_{\mathrm{dev}} = A\mathrm{e}^{\frac{-E}{RT_{\mathrm{prt}}}} \tag{3}$$

and therefore neglects the devolatilization's heating rate dependency. The coal specific pre-exponential factor $A = 1.175 \times 10^6$ 1/s and the activation energy $E = 7.375 \times 10^4$ J/mol have been determined by the CPD model utilizing a heating rate derived from single particle simulation.

2.1.2. Particle heat balance

The equation describing the change of particle temperature assuming homogeneous temperature inside the particle, can be derived from balancing the heat transfer on the particle surface and the change of thermal energy

$$c_{p,\mathrm{prt}} m_{\mathrm{prt}} \frac{dT_{\mathrm{prt}}}{dt} = \dot{q}_{\mathrm{prt,dev}} + \dot{\Psi}_{\mathrm{prt},c} + \dot{\Psi}_{\mathrm{prt},r}. \tag{4}$$

Here, the energy required for the devolatilization process is denoted by $\dot{q}_{\mathrm{prt,dev}}$ on the right hand side of the equation. The term $\dot{\Psi}_{\mathrm{prt},c}$ accounts for the convective energy exchange

$$\dot{\Psi}_{\mathrm{prt},c} = \frac{6\lambda Nu}{\rho_{\mathrm{prt}} c_{p,\mathrm{prt}} d_{\mathrm{prt}}} (T_{\mathrm{g}} - T_{\mathrm{prt}}) \left(\frac{B_h}{\exp(B_h) - 1} \right). \tag{5}$$

Herein, the Nusselt number Nu is calculated from the Ranz-Marshall correlation [52], $Nu = 2 + 0.552 Re_{\mathrm{prt}}^{0.5} Pr^{0.333}$,

Table 1
Parameters for the C2SM model.

$Y_{\mathrm{Vol},0}$ (-)	A_1 (s^{-1})	A_2 (s^{-1})	E_1 ($\frac{J}{mol}$)	E_2 ($\frac{J}{mol}$)	α_1 (-)	α_2 (-)
0.5494	1.54×10^5	2.31×10^7	5.96×10^4	1.0×10^6	0.41	0.75

with $Pr = 0.7$. The heat transfer number is computed as $B_h = c_{p,g}\dot{m}_{\mathrm{prt}}/(2\pi d_{\mathrm{prt}}\lambda)$.

The term $\dot{\Psi}_{\mathrm{prt},r}$ accounts for the radiative energy exchange

$$\dot{\Psi}_{\mathrm{prt},r} = \frac{6\sigma\epsilon_{\mathrm{prt}}}{c_{p,\mathrm{prt}}\rho_{\mathrm{prt}}d_{\mathrm{prt}}}\left(T_{\mathrm{wall}}^4 - T_{\mathrm{prt}}^4\right), \tag{6}$$

where, the wall temperature T_{wall} is assumed to be the burner enclosure with glass walls and constant at 500 K and the particle emissivity ϵ_{prt} is 0.7. σ is the Stefan-Boltzmann constant and is equal to 5.6×10^{-8} W/(m^2K^4). The particle heat capacity is calculated based on the models and approximations by [53,54]. The correlation developed by Merrick [53] is the only self-contained method to calculate the heat capacity of a coal sample. The correlation calculates the temperature-depend heat capacity of the particle based on the volatile, char, and ash fractions.

2.2. Combustion modeling

To consider chemical reactions, species mass fractions Y_i and temperature equations are solved assuming unity Lewis number for all species [21,55].

$$\frac{\partial \rho_g Y_i}{\partial t} + \frac{\partial}{\partial x_\beta}\left(\rho_g\left(U_{g,\beta} + V_{\beta,i}\right)Y_i\right) = \omega_i + \dot{S}_{Y_i} \tag{7}$$

$$c_p\frac{\partial \rho T_g}{\partial t} + c_p\frac{\partial \rho U_\beta T_g}{\partial x_\beta} = -\rho\frac{\partial T_g}{\partial x_\beta}\sum_{i=1}^{N_{sp}} C_{p,i}Y_iV_{\beta,i} + \frac{\partial}{\partial x_\beta}\left(\lambda_g\frac{\partial T_g}{\partial x_\beta}\right) - \sum_{i=1}^{N_{sp}} h_i\omega_i + \dot{S}_T. \tag{8}$$

Gas-phase chemistry is modeled using finite-rate chemistry adopting a specially designed mechanism for coal and biomass combustion with 68 species and 906 reactions [56], which has been validated for the oxidation of different fuels in both air and oxy-fuel atmospheres. Moreover, the gas-phase equations include source terms to represent the particle interaction, which can be seen by $\dot{S}_T$ for the temperature equation and $\dot{S}_{Y_i}$ for the species transport, respectively.

2.2.1. FGM modeling

Since the utilization of finite-rate chemistry with detailed mechanisms is limited to generic test cases for complex fuels like coal, detailed mechanisms are also used in the framework of Flamelet Generated Manifolds (FGM). The primary development of the FGM modeling approach was done by van Oijen et al. [57] and was recently extended for pulverized coal combustion [10,11,25,48]. To obtain the FGM table, laminar premixed flames are calculated using the 1D detailed chemistry flame solver Chem1D [58] applying a unity Lewis number assumption for all species. The approach was previously successfully applied and validated for single-particle ignition and combustion by Knappstein et al. [10,25]. Considering combustion chambers, where mixing of the released matter from multiple particles and reactions coincide, multi-regime characteristics become important, as for example shown by Wen et al. [16]. In the case of combustion in particle group configurations, the released volatiles undergo strong mixing leading to homogeneous mixtures entering the flame front. Since both mixture fraction and reaction progress are varying during this progress, both non-premixed and premixed tables have advantages and disadvantages and none of them is clearly superior to the other. However, for increasing particle number densities, the homogeneity of the mixture increases before entering the flame. Therefore, the application of premixed flamelets constitutes a reasonable approximation.

The progress variable is defined as a combination of the mass fractions of Y_{CO_2}, Y_{CO}, and Y_{O_2}. Since the focus in this study is mainly on the ignition and volatile combustion, and char oxidation and gasification, which need longer residence times, are not considered as they would need additional mixture fractions in the context of tabulated chemistry. A generalized two mixture fraction approach developed in a previous study [11] that can differentiate between methane and volatiles is applied here. The first mixture fraction Z_{FF} describes the mixing of methane with the oxidizer [25]. The second mixture fraction $Z_{\mathrm{Vol.}} = Z_{\mathrm{C,Vol.}} + Z_{\mathrm{O,Vol.}} + Z_{\mathrm{H,Vol.}}$, which is defined as the sum of the element mass fractions of C, O, and H from volatiles, characterizes the mixing of volatiles with the oxidizer. As the mixture fraction composition must be known before the simulation, a fixed composition is mandatory. Otherwise, mixture fractions for each species, that is released separately from the particle would be needed, which is not feasible due to current memory restrictions. The computations of the flamelets must be repeated for all mixture fractions within the flammability limits. Outside the flammability limits, an interpolation technique assuming pure mixing is adopted [25]. To represent heat transfer in the table, the flamelet calculation is repeated for different enthalpy levels. A detailed description of the table generation process is given in [11].

By pre-calculating flamelets, only equations for the trajectory variables have to be solved. Moreover, the species source terms can be directly taken from the table. In the context of flamelet modeling, instead of the temperature equation, the enthalpy equation

$$\frac{\partial \rho h}{\partial t} + \frac{\partial \rho U_\beta h}{\partial x_\beta} = \frac{\partial}{\partial x_\beta}\left(\frac{\lambda}{c_p}\frac{\partial h}{\partial x_\beta}\right) + \dot{S}_h, \tag{9}$$

where $\dot{S}_h$ describes the enthalpy exchange between particles and the gas-phase, is solved. This has the advantage of a constant enthalpy for each flamelet and no source term originating from chemical reactions must be resolved on the numerical grid.

2.3. Interaction of Euler and Lagrange phase

The gas phase and the solid phase are fully coupled using the two-way coupling approach through the source terms appearing in the governing equations at each computational cell with volume Ω_g. In the Eulerian-Lagrangian framework, the particle equations are derived according to the film model, assuming a uniform gas field around the particle. To capture the gas-phase ignition, the domain size is discretized with cubic cells of length dx, which is equal to the diameter of the mono-disperse particles for all simulations [21,29]. Since using the gas phase quantities from grid cells with the same size as the particles is not consistent with the film model assumption, a filter is applied to provide a smoother field in the gas phase to evaluate the state of the gas surrounding the particle consistently with the film model. This approach has been proposed and validated in Ref. [21]. Also, to avoid large particle source terms caused by small cell to particle ratios and to provide grid-independent values, the distribution coefficient ϕ^k

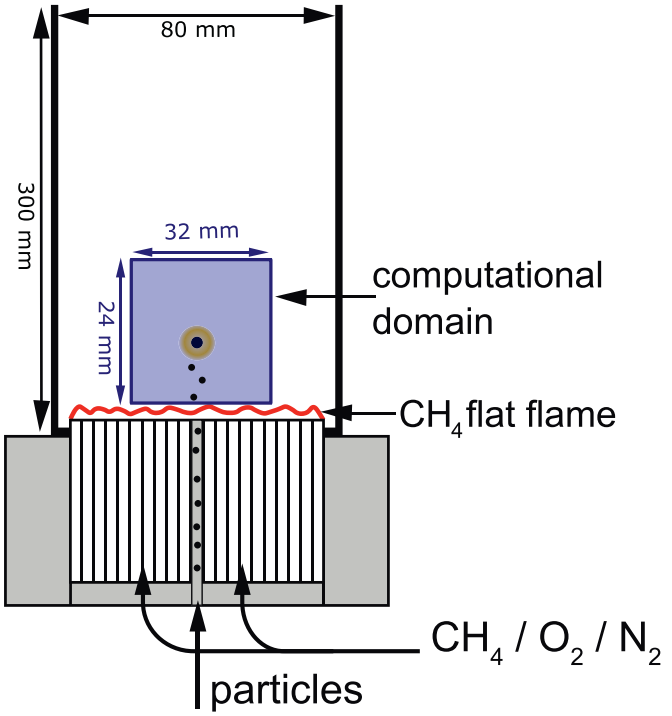

Fig. 1. Schematic cross-section of the flat flame burner. Numerical domain used for the simulations is highlighted in the shaded area.

for each particle k is adopted [21,29]. The distribution coefficient is computed by a Gauss function with a characteristic width L_d, centered at the kth particle position. Similar to the distribution length L_d used by Farazi et al. [21,29], L_d is set to 2 d_{prt} where d_{prt} corresponds to the particle diameter. Then, the source terms in the Eulerian equations can be written as

$$\dot{S}_m = -\frac{1}{\Omega_g}\sum_{k=1}^{n_{prt}} \phi^k \left(\frac{dm^k_{prt}}{dt} \right) \tag{10}$$

$$\dot{S}_{U,\beta} = -\frac{1}{\Omega_g}\sum_{k=1}^{n_{prt}} \phi^k \left(\frac{dm^k_{prt}}{dt} U^k_{prt,\beta} + m^k_{prt} \frac{dU^k_{prt,\beta}}{dt} \right) \tag{11}$$

$$\dot{S}_{Y_i} = -\frac{1}{\Omega_g}\sum_{k=1}^{n_{prt}} \phi^k \left(\frac{dm^k_{prt,dev,i}}{dt} \right) \tag{12}$$

$$\dot{S}_T = -\frac{1}{\Omega_g}\sum_{k=1}^{n_{prt}} \phi^k \left(\frac{dm^k_{prt}}{dt} c^k_{p,prt} T^k_{prt} + \dot{\Psi}^k_{prt,c} \right) \tag{13}$$

$$\dot{S}_h = -\frac{1}{\Omega_g}\sum_{k=1}^{n_{prt}} \phi^k \left(\frac{dm^k_{prt}}{dt} h^k_{vol} + \dot{\Psi}^k_{prt,c} \right) \tag{14}$$

3. Experimental configuration and numerical setup

3.1. Experimental setup and optical measurements

The optical measurements were performed in an enclosed flat flame burner (FFB) depicted in Fig. 1. Due to its excellent optical access, well-defined boundary conditions are available from measurements. For further details on the setup and configuration of the FFB, the reader is referred to previous works [19,20]. Coal particles were seeded through an injection tube with an inner diameter of 0.8 mm.

Regarding the bituminous coal investigated in this work, numerous experimental works from different groups have evidenced the dominance of the homogeneous ignition mode [17,18,59,60]. Moreover, previous experimental studies also showed homogeneous ignition in oxidizing environments [19,20,61,62]. The particle sizes used in these studies ranges from 40 to 200 μm, in N_2 or CO_2 with oxygen from 5% to 40%. It indicates that the ignition mode is less sensitive to particle size and oxygen enrichment but is impacted mainly by the coal rank and particle heating rates. Hence, the chosen setup represents an appropriate choice for the comprehensive study of sub-models required for homogeneous ignition as the occurrence of heterogeneous ignition is improbable for the selected boundary condition.

The optical setup is schematically illustrated in Fig. 2 and was extensively described elsewhere [28]. Laser scanning utilizing an acousto-optic deflector (AOD) has been demonstrated in turbulent gaseous flames [63] and was implemented for the present application in solid fuel combustion. The ignition of the volatile flame associated with particle groups was experimentally determined by the high-speed volumetric laser-induced fluorescence of the hydroxyl radical (OH-LIF). The OH-LIF setup consisted of a dye laser system tuned to an output wavelength of 283.01 nm, a laser scanner, and an intensified CMOS camera for signal detection. The field of view of OH-LIF covered the region in which homogeneous ignition occurred and the volatile flame developed. Every ten successive planar images were used for a signal reconstruction within a 3D volume of 18.7 × 18.7 × 3.8mm^3. The ignition height was determined by using a normalised OH-signal image with fixed threshold of 1.4, which dealt with the fluctuation of the background intensity of the flat flame flue gas. By evaluating the particle velocity profiles for differently loaded particle jets using the diffuse backlight-illumination (DBI) measurements, the ignition delay time with respect to the start of the heating (i.e., particle crossing the flat flame) was derived.

A DBI system consisting of a CMOS camera and a high-power LED was operated at 10kHz to measure the *in-situ* particle number density (PND) and particle velocity profiles simultaneously. The DBI system imaged particle shadow signals up to 13.7mm above the burner surface with a high spatial resolution. After the binarization of DBI images, a particle jet was computed by applying a fixed threshold on the mean DBI image, which included 95% of all particles within its boundaries. The particle velocity was evaluated employing time-resolved DBI image sequences using a combined PIV-PTV approach (Davis 10, LaVision). The statistical evaluation was conditioned both on the PND and the axial-positions of the particle jet. For more details about the experimental methodology and data processing steps, the reader is referred to [28].

3.2. Numerical setup and boundary conditions

This study focuses on the region of ignition. Therefore, simulations were performed within the region with the physical size of 24mm × 32mm × 32mm shown in Fig. 1. The domain is discretized with a three-dimensional Cartesian mesh with a resolution $\delta x = \overline{d}_{prt}$ in the center of the domain and is slightly stretched outward. The total grid consists of about 4×10^6 cells. Gas composition and temperature at the inlet of the simulation domain were adjusted according to the flue gas composition of the flat flame, which was calculated from a freely propagating premixed flame with an unburned temperature of 300 K, an equivalence ratio of 0.56, and a constant coflow velocity to stabilized the premixed flame. The results of the flame calculation are shown in Table 2. The 10% oxygen condition after the FF is chosen due to its high relevance for the local conditions in real configuration. Particularly in the quarl region, where the recirculated flue gas is mixed with the fresh oxidizer, fuel-rich mixtures with low oxygen concentrations

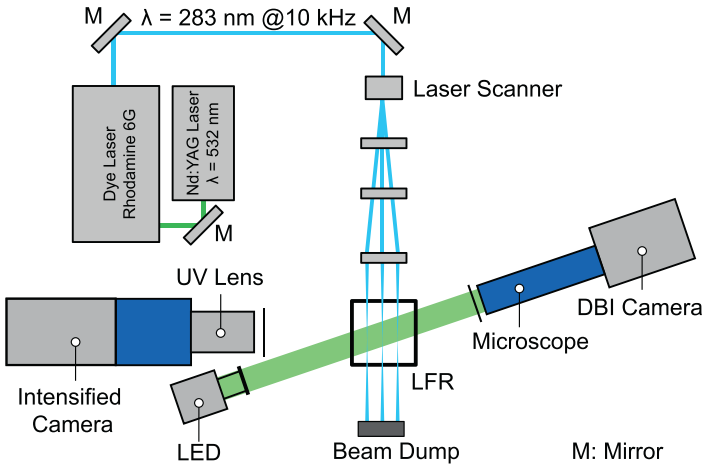

Fig. 2. Sketch of the experimental setup of simultaneous OH-LIF and DBI measurements.

Table 2
Operating conditions for the FFB.

	Inlet	After FF
CH_4	0.068	0.0
O_2	0.236	0.1
N_2	0.696	0.696
CO_2	0.0	0.0685
H_2O	0.0	0.1355
ϕ	0.56	

Table 3
Coal properties of Colombian Norte.
1: as received, 2: dry and ash free basis

Proximate analysis[1]	wt. %
Moisture	3.5
Ash	8.7
Volatile Matter	36.9
Fixed Carbon	50.9
Ultimate analysis[2]	**wt.%**
Carbon	78.6
Hydrogen	5.3
Oxygen	13.7
Nitrogen	1.4
Sulfur	1.0

can be found. This has been demonstrated in recent large scale simulations [12,64–66]. In this study, regions with oxygen concentrations similar to that of the fresh gas down to nearly no oxygen have been identified in the region where volatile ignition occurs.

The experiment was carried out with a high-volatile bituminous Colombian coal, with the composition given in Table 3. The experimentally determined mean diameter $\bar{d}_{\mathrm{prt}}$ of 120 μm is used as an input in the numerical simulations to generate particles positioned according to the distribution given by the shadowgraphic measurements directly behind the flat flame. For the current study, simulations with ascending particle injection rates were performed to study the effect of group combustion. For reference, one single-particle case is studied as well. The initial velocity of the particles is given by the time-resolved DBI measurements at the first measurement location behind the flat flame and is dependent on the particle mass flow. As reported in Li et al. [28], the two main reasons for lower axial velocity with increasing particle rates are that particle-particle and particle-wall collisions reduce the kinetic energy of particle group in the injection tube as well as a weaker thermal expansion of gas due to lower gas temperatures in the post-FF region. The particles are assumed to be injected directly into the hot gas stream with the boundary conditions based on Table 4 for single-particle configuration (SP) and particle group configuration (GP). The coal type, atmosphere, and surrounding gas temperature are the same in the single-particle and particle group simulations in order to be able to link the single-particle analysis to the particle group investigation.

4. Results

Several simulations with different combinations of devolatilization and chemistry modeling were conducted in this study to investigate the effect of model reduction for particle group ignition. The comparison of detailed kinetics against tabulated chemistry represented by the FGM model will demonstrate the influence of gas-phase chemistry treatments in the investigated configuration. Also, different levels of detail of devolatilization models are considered in the comparison to assess the accuracy of different devolatilization models. An overview of the model combinations considered in the simulations is given in Table 5.

4.1. Validation

Matching the ignition delay times between simulations and experiments is very challenging and it is always susceptible to both modeling errors and uncertainties in the ignition delay definition. In the experiment, the measured OH signals are normalized to the local intensity originating from the hot exhaust gas of the flat flame before a threshold of 1.4 is applied to define the homogeneous ignition onset. However, the threshold calculation can not be directly applied to the simulation due to the non-linear dependency of OH signals with the OH mass fraction. Therefore, three different thresholds of 10%, 20%, and 30% of OH maximum mass fraction are considered in simulations. Based on these, mean and standard deviations of the ignition delay are computed to allow for consistent comparisons with experiments.

Since in experiments particles are injected randomly in time and space, the average particle injection rate $\dot{N}_{\mathrm{inj}}$ and particle velocity $U_{\mathrm{prt,in}}$ in the simulations are imposed at the inlet such that they are consistent with the experimental boundary conditions. Depending on the particle injection rate, the number of particles in the domain increases until time t_{SSS} when the first injected particles leave the domain through the outlet. For $t > t_{\mathrm{SSS}}$, the system quickly reaches a statistically steady state. After reaching steady-state, the ignition delay time is calculated based on the

Table 4
Injection properties of particles for one single-particle setup (SP) and four particle group configurations with ascending particle mass flows (GP1-GP4).

	SP	GP1	GP 2	GP 3	GP 4
Injection rate (1/ms)	-	1	3	6	9
Mean axial velocity (m/s)	0.74	0.62	0.48	0.4	0.35
Axial velocity fluctuations (m/s)	0.0	0.1	0.1	0.1	0.1
Radial velocity (m/s)	0.0	± 0.04	± 0.03	± 0.025	± 0.02
Particle temperature (K)	300	300	300	300	300

Table 5
Model combinations for the simulations considered in this work.

Case	Dev. model	Vol. Comp.	Gas chemistry model	Particle Injection
A.0-A.4	CPD	dynamic	Detailed kinetics (FC)	SP;GP1-GP4
B.0;B.3	CPD	fixed	Detailed kinetics (FC)	SP;GP3
C.0-C.4	CPD	fixed	FGM	SP;GP1-GP4
D.0-D.4	C2SM	fixed	FGM	SP;GP1-GP4
E.0-E.4	SFOR	fixed	FGM	SP;GP1-GP4

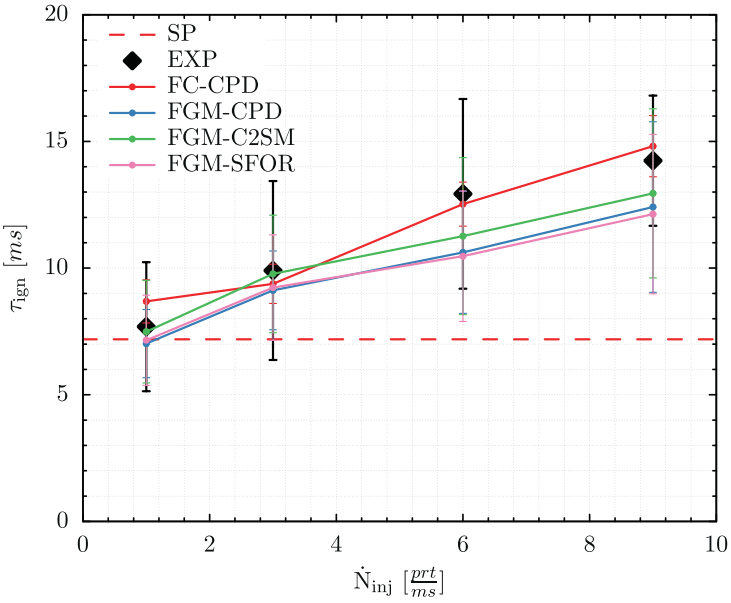

Fig. 3. Comparison of ignition delay time τ_{ign} between experiments (black diamonds with error bars) and A-cases, which are reference numerical simulations (FC-CPD), for different particle injection rates $\dot{N}_{inj}$. The horizontal dashed line (SP) indicates the experimentally measured single-particle ignition delay as a reference. The error bars in the detailed model correspond to different thresholds of Y_{OH}. Flamelet simulation results with different devolatilization models are also shown for C-cases(FGM-CPD), D-cases(FGM-C2SM), and E-cases(FGM-SFOR), respectively.

ignition position and the averaged particle velocity as

$$\tau_{\mathrm{ign}} = \frac{x_{\mathrm{ign}}|_{Y_{\mathrm{OH}}}}{\langle \bar{U}_{\mathrm{prt}} \rangle|_{0<x<x_{\mathrm{ign}}}}. \tag{15}$$

This approach is consistent with the measuring procedure of the ignition delay time in the group combustion experiments and previous numerical simulations [11,28].

Fig. 3 depicts the comparison of ignition delay times between simulation and experiments for different particle injection rates reported in Table 4. Experimental data scatter within two standard deviations indicated by error bars, which mainly resulted from a broad particle diameter distribution and the non-stationary particle mass flow rates. In addition to the detailed simulation, various simplified model combinations (see Table 5) using different devolatilization models are considered to investigate the effects of model simplifications on the ignition delay times.

Comparing the detailed simulation results (FC-CPD) and the experimental data, excellent agreement is observed, which shows the accuracy of detailed simulations in predicting ignition delay time. In the experiments, the line-of-sight particle flow measurements and nonlinear dependency of OH-LIF signals with OH mass fraction are the primary sources of uncertainty. In the FC-CPD simulations, the model parameters for the CPD model are interpolated as the C-NMR data for the employed coal are not available and therefore are obtained from an empirical correlation. Also, particles are assumed to be homogeneous spheres, which leads to uncertainty in the detailed simulations.

The FGM model coupled with the most detailed devolatilization model (FGM-CPD) shows a similar agreement with respect to the ignition delay time as the detailed simulation (FC-CPD). However, a slight underprediction of ignition delay time is observed in FGM results compared to detailed simulations, especially at higher injection rates. It is interesting to note that the FGM model coupled with simpler devolatilization models (FGM-C2SM and FGM-SFOR) also predicts the correct ignition delay time. These results are expected for both models at low injection rates as the model coefficients are fitted using CPD single-particle results. However, SFOR and C2SM still match the experimentally measured ignition delay times reasonably well for higher particle injection rates, although the respective conditions are not explicitly included during

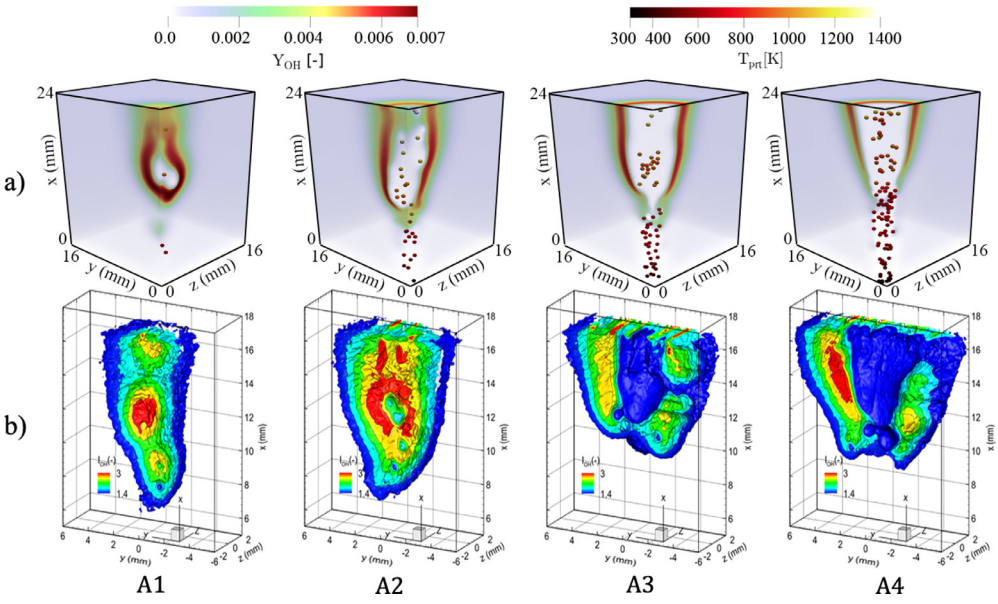

Fig. 4. a) Instantaneous field of OH mass fraction and particle temperature after steady-state conditions showing different flame shapes in the coflow jet configuration, which is the effect of different particle number densities based on the cases in Table 5 compared with b) experimental 3D OH-LIF signals for the corresponding different particle injection rates in the simulations [28].

model fitting for the SFOR model. This observation indicates that well-fitted devolatilization models can capture the ignition behavior of particle group ignition correctly, which was also previously observed in other studies [12,22].

4.2. Effect of injection mass flow rate on volatile combustion

The observations in Fig. 3 show that increasing particle injection rates leads to an increase in the ignition delay time. This difference originates from the changes in the combustion chemistry and particle interactions with the gas phase, which will also lead to different flame structures. As shown in Fig. 1, particles are injected from a circular nozzle in the center of the domain into a hot ambient gas. After reaching the statistically steady-state condition, the flame shapes for different particle injection rates are compared to the experimental observations. As shown in Fig. 4, the clipped 3D OH fields in the simulations have been qualitatively validated with the corresponding 3D OH-LIF measurements in the studied domain for different particle injection rates. The similar qualitative trends for the transition from single-particle ignition to a conical flame structure show that the physical behavior can also be fully captured in detailed simulations (see A-series in Table 5). The same flame structure between the FGM models and the experimental results were observed in the previous study by Nicolai et al. [11], which showed that the FGM model can fully capture the physical behavior of volatile flames associated with particle group combustion.

Comparing all cases spanning the range from low to high injection rates, an increase in ignition height can be found. This qualitative observation corresponds to experimental and numerical findings in the literature [11,27,28]. It is observed that for low particle injection rates, the volatiles mainly burn in spherical flames formed around individual particles, similar to the single-particle behavior observed by Farazi et al. [21]. A transition from a spherical flame around individual particles with higher OH concentrations to a more continuous flame region around particle groups with lower OH concentrations is observed by increasing the particle injection rate. Due to the presence of multiple particles, the energy demand for particle heating increases significantly for higher injection rates. This leads to substantial cooling of the hot surroundings and, as a consequence, lower rates of particle heating and devolatilization, which causes delayed ignition.

As shown in Fig. 5a, after injection, due to the energy transfer required for particle heating, the gas temperature T_g drops in the vicinity of the particles along the stream-wise direction (jet centerline) before the ignition location is reached [29]. For the high-volatile bituminous coal, devolatilization begins with releasing a small amount of light gases, which accelerates at higher temperatures when the release of tars starts. Moving further downstream, at a certain distance from the inlet for each case, volatile ignition happens where the gas temperature T_g begins to increase. It is observed that injecting a higher number of particles requires a higher amount of energy for particle heating and shows a more significant temperature drop in the gas phase, as shown in Fig. 5a. This strong cooling effect at the particle location for higher particle injection rates leads to lower gas temperatures at the centerline. For case A4, the temperature becomes so small that because of the high activation energies of the reaction, the ignition process is suppressed in the region around the centerline. Additionally, when comparing Y_{O_2} at the centerline, it is observed that for higher particle injection rates, local oxygen deficiency, which leads to low oxidizer to fuel ratios, results in a suppression of volatile ignition in that region [11]. However, a comparison of the radial profiles of the gas temperatures after ignition (see Fig. 5b) shows that for higher particle injection rates, the gas temperature increases at farther distances from the centerline and reaches its peak at a certain distance, where ignitable mixtures are formed due to the mixing of volatiles with the oxidizer. Comparing all cases from low to high injection rates, the peak temperature moves further away from the centerline, indicating the opening of the jet-like flame.

The energy transfer between particles and the surrounding hot gas increases the particles' temperature. As a result, thermal decomposition and, consequently, devolatilization occur when particles approach a certain temperature. As shown in Fig. 6, a slowed increase of T_{prt} is observed for higher particle injection rates, since denser streams with an overall higher mass demand significantly more energy for particle heat-up, which leads to lower particle heating rates. It should be mentioned that since the state of combustion is controlled by the experimental boundary conditions in order to capture the ignition and flame transition

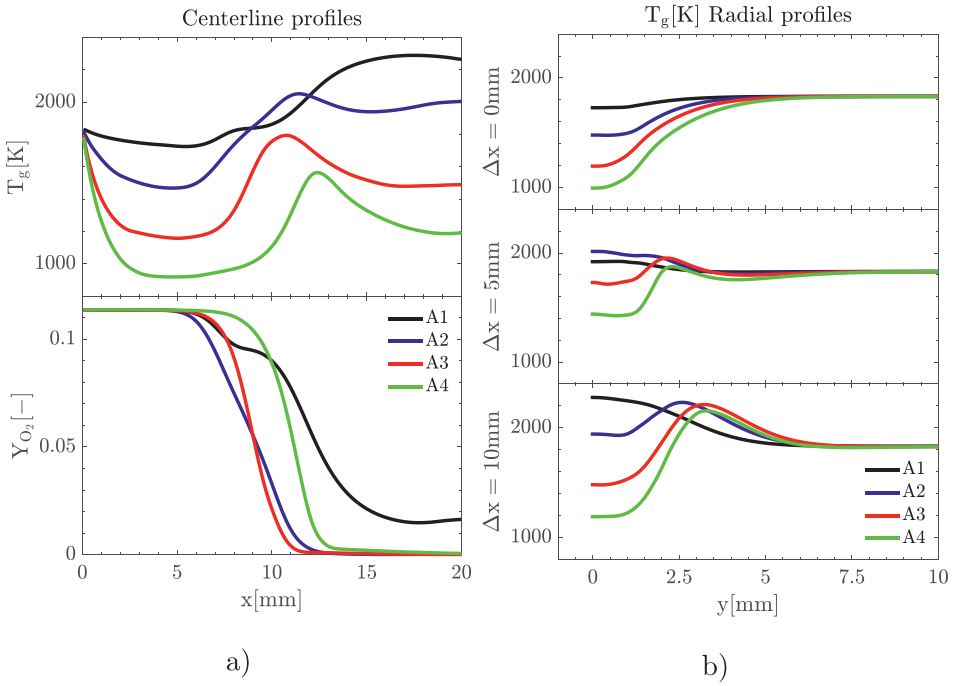

Fig. 5. (a) Axial profiles of the time-averaged gas temperature (T_g) and O_2 mass fraction along the jet centerline, and (b) radial profiles of the time-averaged gas temperature at different relative heights (compared to ignition height) for different injection rates (see Table 5).

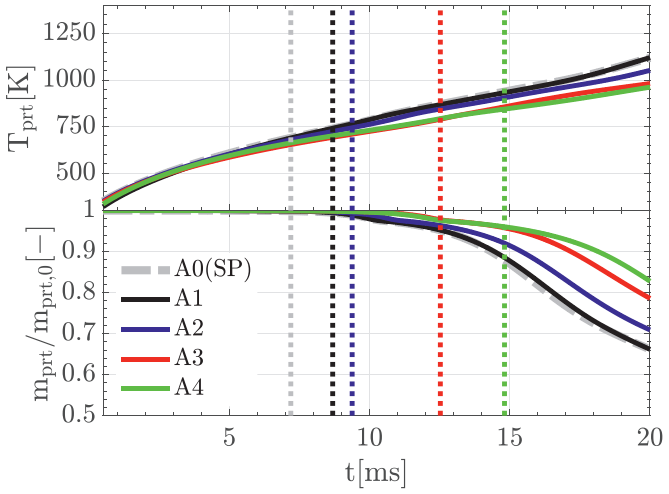

Fig. 6. Maximum particle temperature (T_{prt}) and particle normalized mass ($m_{prt}/m_{prt,0}$) for single-particle (SP) and particle group (A-series) combustion (see Table 5), in which the ignition times are shown with dotted lines.

from single-particle to particle group combustion within the flammability limit, only a limited range of particle heating rates could be simulated, which for cases from the lowest injection rate (A0) to the highest injection rate (A4) varies between the range of 45,000–60,000 K/s. The slower evolution of the particle temperature due to lower heating rate leads to an overall lower thermal decomposition of the particle structure and, consequently, a delay in volatile release and a lower overall mass loss. However, the continuous volatile release in denser streams causes a change in the flow dynamics around the jet, which leads to a radial shift of the flame towards the outer ambience where fuel is fully burned and sufficient quantities of O_2 remain to support combustion.

With regard to combustion chemistry, as shown in Fig. 4, it is observed that increasing the particle injection rate leads to a decrease in Y_{OH}. Lower OH production decreases the reactivity of the mixture, which is consistent with the delayed ignition for higher particle injection rates. This is investigated via a reaction pathway analysis of the intermediate reactions and their corresponding reaction rates similar to the study by Farazi et al. [21]. Therefore, different species profiles along with the location of the peak OH value in the domain (peak reactivity region) are studied. As shown in Fig. 7, by increasing the particle injection rate, higher CO_2 concentrations at the peak reactivity region are observed. Higher CO_2 concentrations cause a stronger depletion of H radicals by reaction R1: $CO_2 + H \rightarrow CO + OH$. In particular, reaction R1 produces an OH radical by the consumption of an H radical and does not affect the radical pool. However, a depletion of H radicals reduces the reaction rate of the main chain branching reaction R2: $O_2 + H \rightarrow OH + O$. In this reaction, two radicals are formed and, in particular, the O radical eventually forms two OH radicals via the reaction R3: $H_2O + O \rightarrow 2OH$. Thus, the increased depletion of H radicals via reaction R2 for higher injection rates leads to an overall reduction of the radical pool. In addition, concentrations of O_2 are reduced for higher injection rates, which further reduces reaction rates of reaction R2, leading to the overall lower OH production.

4.3. Model simplification

Since quantitative information from experiments is limited for model assessment, detailed simulations are required to investigate the source of uncertainties and study the effects of simplifying assumptions. In order to fill the gap between the detailed simulations and the simple models for pulverized coal volatile combustion, a systematic model reduction approach is used in the current study. The model reduction is separated into three major steps.

First, the effects of a simplified volatile composition assumption are investigated. In most simplified coal combustion modeling approaches, especially for flamelet models, it is required to assume a fixed volatile composition in time as mentioned above, see Section 2.2.1. This assumption may be susceptible to uncertainties based on the volatile release process. Detailed devolatilization models, such as the CPD model, show that volatile composition,

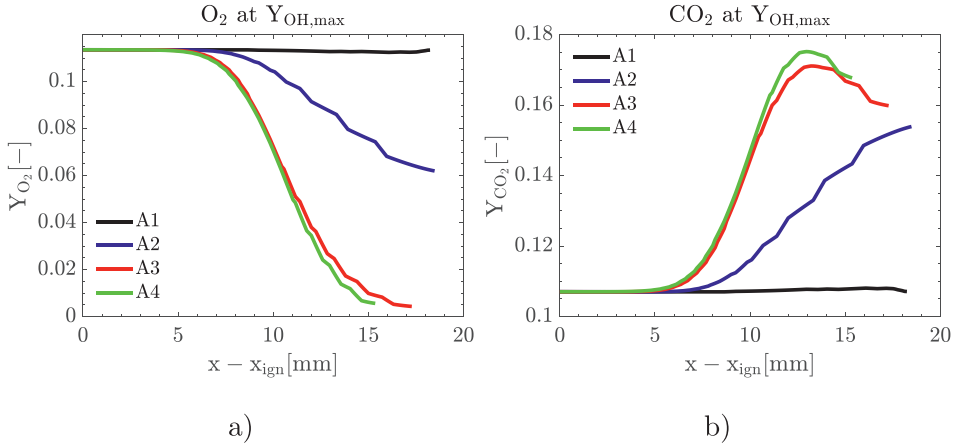

Fig. 7. Mass fractions of O_2 and CO_2 along the location of $Y_{OH,max}$ (peak reactivity region) at relative distances to ignition position (x_{ign}) for different particle injection rates (A-series in Table 5).

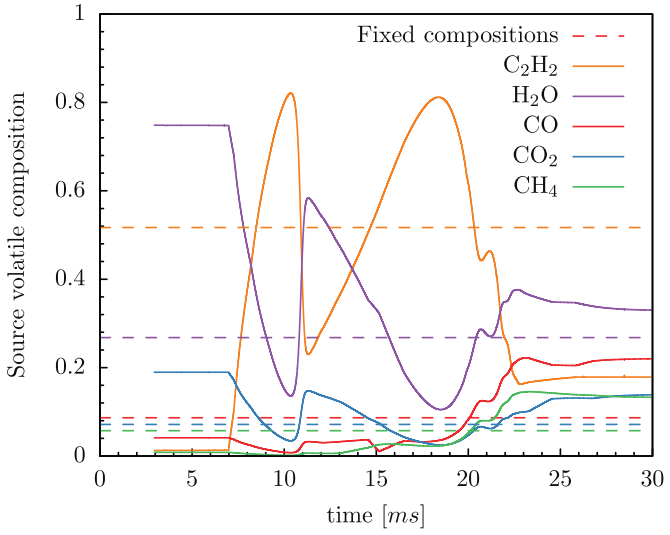

Fig. 8. Source volatile composition prediction of the dynamic volatile composition (reference) model compared to a fixed volatile composition assumption.

especially tars, will significantly change during devolatilization [21], questioning the fixed volatile composition assumption's accuracy. This assumption is tested in the detailed simulation framework using detailed kinetics coupled with the CPD model in the single-particle and particle group configuration to assess its accuracy in the ignition and combustion chemistry predictions.

In the next two steps, the model is further simplified by using FGM coupled with different models with varying levels of detail for devolatilization, where CPD, C2SM, and SFOR models are used for comparison. The effect of gas-phase chemistry on ignition and combustion chemistry is investigated by comparing results from detailed kinetics and tabulated chemistry using the same devolatilization model (CPD). Finally, using the FGM model, the effects of different devolatilization models on ignition and combustion chemistry predictions are assessed. The accuracy of the simplified model is investigated based on the reference case results.

4.3.1. Effect of volatile composition on ignition and combustion

To study the effects of the volatile composition, a case assuming fixed volatile composition (FVC) is simulated, in addition to the previously discussed detailed reference case. Fig. 8 shows the differences between the prediction of the source volatile composition in the dynamic model compared to FVC. The fixed volatile composition is calculated based on the time-averaged values of each volatile species' mass compared to the total released mass from the particle. These modeling steps are accompanied by two assumptions, which might affect homogeneous ignition and combustion: The species are released with the same composition during devolatilization, and the heating value of the volatile species remains constant over time. This can lead to discrepancies between the volatile species predicted by the devolatilization model and those released to the gas-phase. The influence of these modeling assumptions, which are always present when simpler devolatilization models are applied, is investigated in the following.

To investigate the effects of model simplification in particle group combustion, it is required first to study the basis of the model simplification in a simpler configuration, where the effect of volatile flame interactions in group combustion is not present. Therefore, single-particle ignition and combustion is compared for cases A0 and B0 described in Table 5.

As Fig. 9 shows, using the FVC assumption leads to an overall underprediction of the ignition delay time. In order to investigate the reason for this underprediction, the differences in the particle and the gas phase between the reference case and the FVC model are studied. As shown in Fig. 9a, since the particle temperature and normalized mass loss, which represents the volatile release rate, are the same in the reference simulation and the FVC model, it can be concluded that the volatile composition does not affect the particle thermal decomposition, and the main reason for ignition underprediction in the FVC model is the effect of volatile composition on the gas-phase chemistry. As shown in Fig. 8, different released volatile species in the beginning of the devolatilization in the FVC model, especially higher tar (C_2H_2) and lower H_2O fractions, leads to faster ignition. This different composition has a direct effect on the gas-phase chemistry. Comparing the representatives of radicals (OH) and major species (CO and H_2O) in Fig. 9b shows that before ignition higher OH fractions in FVC model leads to faster ignition. In contrast, after ignition, the FVC model reveals an overall underprediction of major species for the subsequent combustion process.

To include the volatile flame interactions in particle group combustion, the model simplification analysis is extended for comparing the ignition and combustion chemistry in the particle group configuration. Based on Table 5 and Fig. 4, case A3, which shows the flame opening behavior, is selected as a reference for further investigation of the model simplification. To assess the accuracy of the FVC assumption in predicting ignition and combustion chemistry, the same case as for the FVC assumption

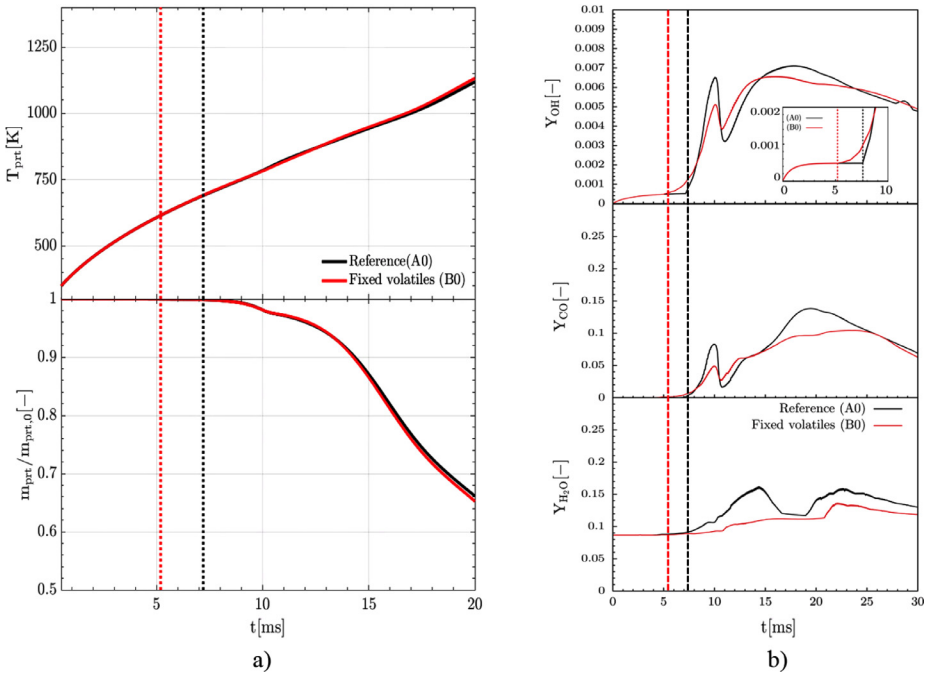

Fig. 9. (a) Comparison between the particle temperature and mass loss ratio, and (b) predictions of the peak OH representing the minor species and radicals, and H_2O and CO mass fractions in the gas phase representing the major species, for the reference case and the FVC model. Dotted lines correspond to the ignition delay times for each case.

Table 6
Effect of the FVC assumption on ignition delay time for single-particle configuration compared to the particle groups configuration

	A0	B0	A3	B3
τ_{ign}[ms]	7.591	5.189	12.048	10.786
e_{ign}[%]	31.6		10.5	

(B3) is simulated, and the differences in the prediction of ignition delay time and combustion chemistry are compared to the single-particle configuration.

As shown in Table 6, an overall lower ignition delay time is also observed in the particle group configuration comparing the FVC model with the reference case. However, comparing the relative prediction error in ignition delay times (e_{ign}) in particle groups compared to the single-particle configuration, it is observed that the FVC assumption leads to a smaller relative difference in ignition delay time for particle groups. The reason for the smaller discrepancies in the particle group configuration compared to the single-particle configuration is that in the presence of multiple particles, two main characteristics are changing in the gas phase. On the one hand, the released volatiles from particles are exposed to strong mixing processes with the volatile gases of the other particles. On the other hand, the strong heat losses in the gas phase as a consequence of heating multiple particles lead to lower gas-phase temperatures. These two effects combined are substantially affecting the ignition process by suppressing the early ignition of released light gases by low temperatures. Moreover, the rich mixture formation in the center of the domain facilitates long mixing times of the released volatiles, leading to a homogeneous mixture entering the flame front. This homogeneous mixture can be sufficiently represented by the fixed volatile composition leading to small overall errors compared to single-particle ignition in which the volatile mixing and the strong heat loss effects are not present. The smaller difference shows that the FVC assumption performs better for particle group combustion.

Figure 10 shows the instantaneous and time-averaged OH fields. Due to the jet's axisymmetric geometry, time-average fields have been computed in the central jet plane in the radial direction within a time range after a statistically steady-state condition has been reached. It is observed that the FVC assumption does not affect the flame shape, and only minor differences in the maximum OH values can be observed.

To further investigate the differences in the flame structure between the two cases quantitatively, the averaged fields are computed at different relative heights compared to the ignition point. To assess the accuracy of FVC assumption, the predictions of minor and major species in volatile combustion chemistry are compared with the reference case. Gas temperature (T_g) and heat release rate ($\dot{Q}$) are also considered to evaluate the heating process involved in volatile combustion. As shown in Fig. 11, an overall minor underprediction for OH is observed. Regarding major species, an overall overprediction of O_2, and underprediction of H_2O and CO in the FVC model (B3) compared to the reference case (A3) are observed. Also, relative differences in the gas temperature and the heat release rate predictions are in the same order as the differences between the ignition predictions. This behavior is consistent with the observations for the single-particle configuration.

The most obvious differences between the reference case and the FVC model are observed in the H_2O predictions. One main reason is that H_2O is mainly released at the beginning of the devolatilization process. Using the FVC assumption leads to smoothing of the H_2O release from the particle, which causes the difference in the gas-phase predictions of H_2O. However, the differences occur mostly in the center of the domain, where combustion is suppressed due to oxygen deficiency. In the peak reactivity region, where ignitable mixtures are formed due to the mixing of volatiles with the oxidizer (peak OH positions), differences between the prediction of the major species are also minor. The overall minor difference between combustion chemistry predictions in the reference case and the fixed volatile composition model shows that the assumption of fixed composition and the resulting fixed heating value of the volatiles commonly employed for creating the flamelet manifolds in the FGM modeling is valid to good accuracy.

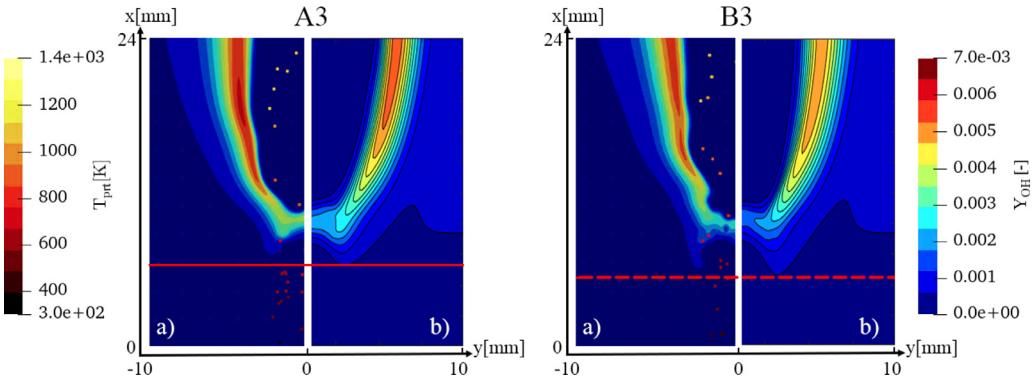

Fig. 10. (a) Instantaneous OH half-fields at t = 70 ms and (b) time-averaged contour plots of OH half-fields for A3: reference case, and B3: FVC assumption. Ignition heights for A3 and B3 are highlighted by the horizontal solid line and dashed line, respectively.

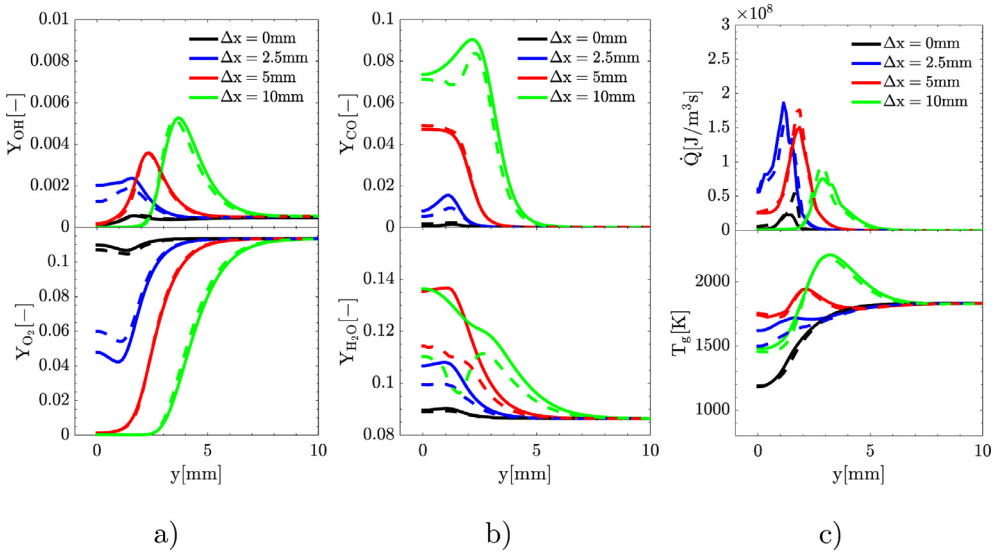

Fig. 11. Radial profiles of the time-averaged fields of a) OH and O_2 mass fractions, b) H_2O, and CO mass fractions, and c) heat release rate and gas temperature, at different heights from the ignition point for the reference case (A3: solid lines) and the FVC model (B3: dashed lines)

4.3.2. Effect of simplified models on volatile ignition and combustion

Next, the influence of the reduction of the gas-phase chemistry and the influence of simpler global devolatilization models (e.g. C2SM and SFOR) on both single-particle and particle group ignition and the subsequent volatile combustion are analyzed. As already shown in Fig. 3, the ignition delay can be correctly predicted by well-adapted C2SM and SFOR models for the conditions considered in this study.

However, as depicted in Fig. 12 by the histories for the particle maximum temperature and normalized mass loss for the single-particle case (Fig. 12 a) and the 6 prt/ms case (Fig. 12 b), the ignition delay is only a marker for the correct initial volatile release, while in the later stage, differences are apparent. For the single-particle case, the particle temperature exhibits the same steep increase for all models. Moreover, the reference solution depicts the same trend for the particle temperature. Regarding the normalized mass loss, differences are visible. After the initial volatile release, mass is released faster using the simplified devolatilization models compared with the CPD model. In the beginning, the reference simulation predicts the same release as the FGM-CPD model, but after 15 ms, the release rate increases due to a somewhat higher particle temperature. Overall, the particle conversion process is similar for all models. The slight difference in the particle temperature before the ignition between the reference model (FC-CPD) and the simplified models originates from the slight differences in the devolatilization prediction between different models.

Due to the increased heat transfer caused by a denser particle stream, the final temperature for the group combustion case is approximately 150 K lower compared to the single-particle case. After approximately 10 ms, all models predict the initial release of volatiles. Although simpler models are fitted utilizing the heating rate of the single-particle CPD simulation, the ignition delay time shows a marginal difference between the simplified models for the particle group combustion. However, for the higher particle injection rate case, differences become apparent with respect to the reference simulation. The reference solution exhibits the longest ignition time, which is likely caused by the dynamic volatile assumption, discussed in the previous section. Moreover, the volatile release rate for all simplified models is higher compared to the reference simulation. The reason for that is the slightly higher particle temperature of the simplified models compared to the reference solution.

To study the influence of the devolatilization model on the subsequent volatile combustion, Figures 13 and 14 depict the profiles of the gas-phase temperature T_g, heat release rate $\dot{Q}$ as well as representative major and minor species at different axial heights

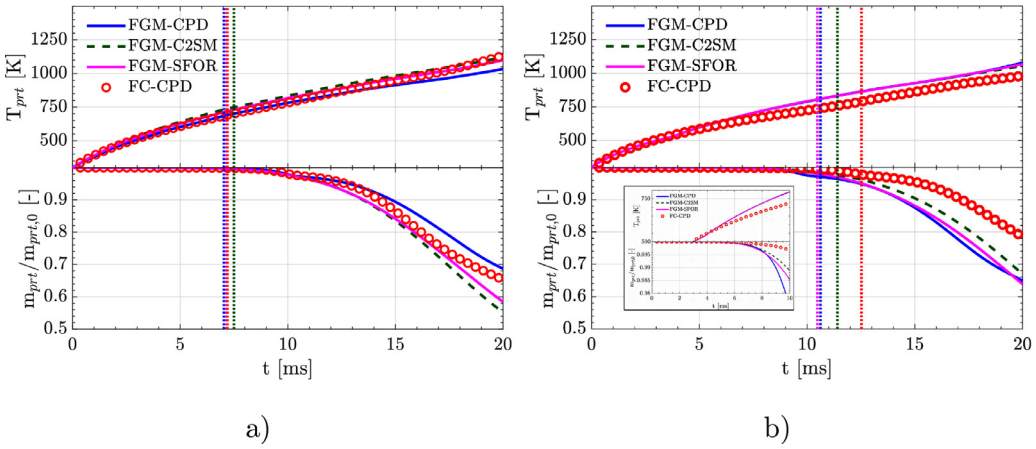

Fig. 12. Histories for the maximum particle temperature T_{prt} (top) and particle normalized mass $m_{prt}/m_{prt,0}$ (bottom); a) single-particle cases C0-E0 b) particle group cases C3-E3. Red circles indicate the reference solution with dynamic volatile release (A cases: FC-CPD).

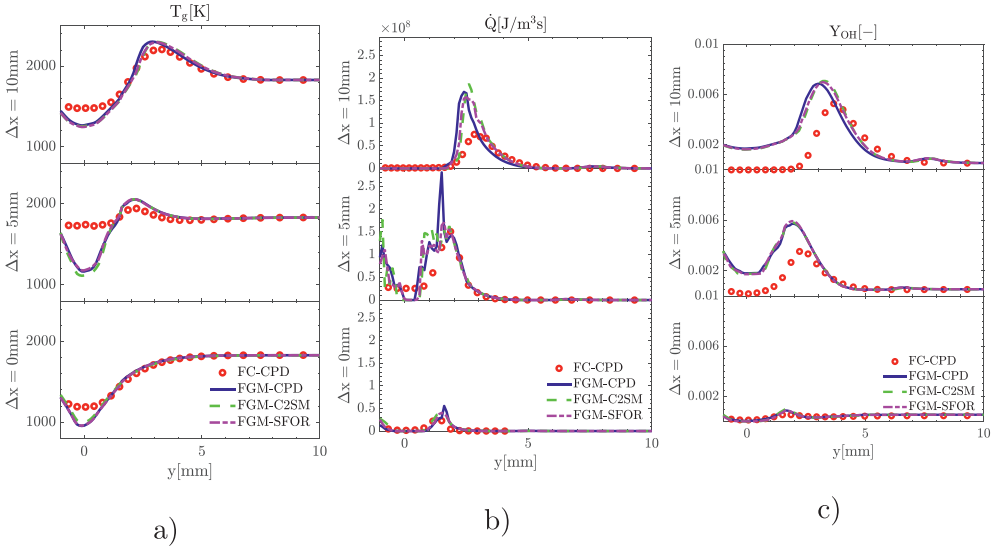

Fig. 13. Radial profiles of mean gas-phase properties for all considered devolatilization models at different axial distances. a) Gas temperature T_g; b) Heat release rate $\dot{Q}$; c) OH mass fraction Y_{OH}. Red dots indicate the reference solution.

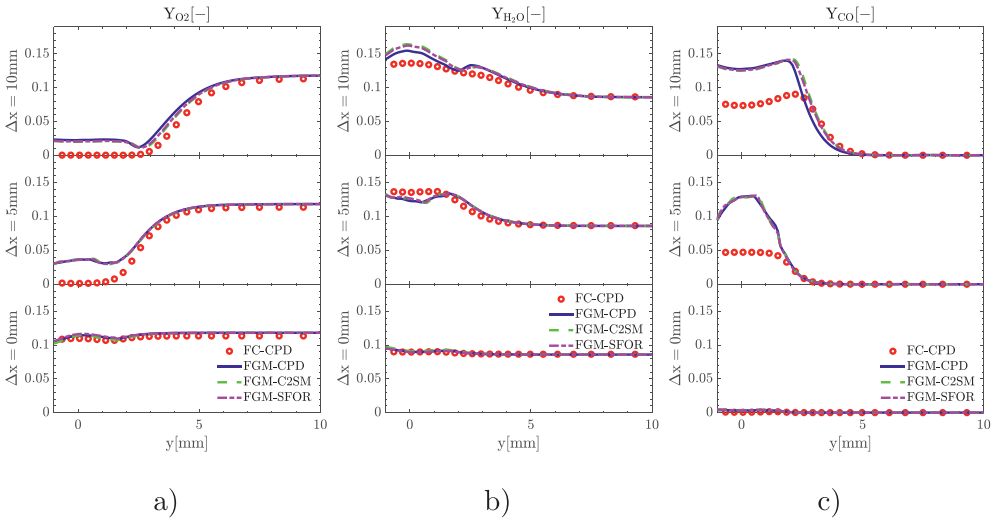

Fig. 14. Radial mean profiles of gas-phase properties for all considered devolatilization models at different axial distances. a) O_2 mass fraction Y_{O_2}; b) H_2O mass fraction Y_{H_2O}; c) CO mass fraction Y_{CO}.

Δx with respect to the ignition height. Despite the differences in ignition delay time, only minor differences between the respective devolatilization models are visible.

At the ignition location $\Delta x = 0$ mm, as expected, marginal changes compared to the inlet composition are visible for the species. However, the temperature shows a significantly lower value in the center of the domain due to strong heat exchange for particle heating. Compared to the reference simulation, slightly lower temperatures can be observed for the simplified global models. This can be explained by the larger ignition delay time of the reference case, which causes the particle and gas-phase to further approach their equilibrium temperature. For the profiles inside the flame, all considered devolatilization models exhibit similar trends. In the center of the domain, the low temperature and rich mixture of volatiles suppress the reaction as indicated by the marginal heat release rate. This causes high CO and low O_2 concentrations in the center. Moving further outside, the temperature peak as well as the OH and heat release rate peak indicate the flame location. Compared to the reference simulations, differences are visible. The temperature profiles show different trends comparing finite-rate chemistry (reference solution) and FGM simulations. While in the FGM simulations, the centerline temperature gradually increases for higher axial distances, the reference simulation shows a high temperature at the $\Delta x = 5$ mm location followed by a lower temperature at $\Delta x = 10$ mm. The reason for these deviations can be explained by reactions outside the flammability, which are not accounted for in the FGM table [10]. For mixtures outside the flammability limits, as mentioned in Section 2.2.1, an interpolation technique is adopted, assuming pure mixing. However, mixing processes between released volatiles and the local mixture around the particle can lead to states beyond the equilibrium state of the table. In the case of finite rate chemistry, chemical reactions will occur if oxygen is left after a sufficient amount of time. In contrast, reaction progress is not included in the FGM table at these states. This mechanism can be identified by small heat release rates in the reference simulation consuming the remaining oxidizer in the center of the domain, leading to higher temperatures and lower CO concentrations compared to the FGM simulation.

Considering the flame position marked by the maximum temperature, the FGM gives favorable results. It is interesting to note that the OH-peak is shifted outwards for the reference simulation, which can be again explained by the fixed volatile assumption. However, all other species in the peak reactivity region show excellent agreement with the reference simulation. Besides the values in the fuel-rich zone inside the volatile flame, the simplified models, regardless of the level of detail of the devolatilization model, predicts the volatile combustion process accurately.

In summary, the investigated models exhibit differences in predicting ignition delay times. However, the chemistry of the particle group's volatile flame is not strongly influenced by the different ignition delay times.

5. Conclusion

This study presented a comprehensive investigation on volatile ignition and combustion of single-particle and particle groups conducted in a flat flame burner. For this purpose, detailed reference simulations, which were successfully validated against the available measurements, were exploited to analyze the physical processes that determine the transition from single to particle group combustion. The data were also used for the detailed assessment of simplified models.

The ignition delay times, as well as the global trend of increasing ignition delay times for higher particle injection rates, showed agreement for all investigated conditions, especially considering uncertainties in both simulations and experiments. Furthermore, the transition from spherical flames around single particles at low injection rates to a continuous conical flame around the central particle group at high injection rates observed by the 3D OH-LIF measurements were correctly captured by the detailed simulations.

The transition's primary causes have been related to the energy transfer between particles and the gas phase and the local oxygen concentration. Also, it has been found that increasing particle injection rates lead to weaker peak reactivity regions in terms of OH peak values, which is due to higher radical depletion by higher CO_2 and lower O_2 in the peak reactivity region.

In addition to the investigation of physical processes, the complete thermo-chemical state has been extracted from detailed simulations, which allows the detailed assessment of reduced-order models for particle group combustion and a comprehensive investigation of each reduction step to evaluate the assumptions involved in pulverized fuel FGM modeling. In the first reduction step, the effects of fixed volatile composition, which is one of the main required assumptions in FGM modeling, has been investigated in the single-particle and particle group configuration. It has been found that using this assumption leads to lower ignition delay times in both configurations due to different volatile compositions and their effect on gas-phase chemistry. However, due to only minor differences in the particle group configuration, FVC is a valid assumption for predicting homogeneous ignition and combustion chemistry.

In the next reduction step, the effects of gas-phase chemistry by comparing the detailed kinetic results with FGM modeling have been investigated. Additionally, to investigate the effect of different devolatilization models in homogeneous ignition and combustion chemistry predictions, three models with varying levels of detail (CPD, C2SM, and SFOR) for the devolatilization process have been considered in the FGM model simulations. The investigation revealed that well-fitted simple models (SFOR, C2SM) can correctly capture ignition delay times. However, as the parameters are quite sensitive to the heating rate, quantitative agreements are very dependent on the heating rates used for fitting the parameters. Only minor differences are visible between the devolatilization models considering the influence on the flame structure. In contrast, the comparison with the reference simulation revealed that the FGM model has some deficits, especially in the domain center, where the mixing processes exceed states tabulated in the FGM table. It was shown that the FGM method could not correctly capture the reactions occurring in this region. However, the flame structure was correctly reproduced with respect to species production, except for an OH shift originating from the fixed volatile assumption.

Overall, this study showed that detailed devolatilization models coupled with finite-rate chemistry could correctly capture the homogeneous ignition and combustion for particle groups. Moreover, the FGM method presents itself as a promising alternative for including detailed gas-phase kinetics at a low cost to compute pulverized coal combustion.

In future works, different oxygen-atmospheres need to be investigated to expand upon this knowledge for particle group combustion in the entire range of operating conditions observed in combustion chambers, including different oxygen concentration and coal types. Moreover, extending the operating conditions to turbulent flows will give new insights into particle group combustion.

Declaration of Competing Interest

The authors declare that they have no known competing financial interests or personal relationships that could have appeared to influence the work reported in this paper.

Acknowledgments

The authors kindly acknowledge financial support through Deutsche Forschungsgemeinschaft (DFG) Projekt nummer 215035359 - through SFB/TRR 129. The authors gratefully acknowledge the Gauss Centre for Supercomputing e.V. for funding this research by providing computing time on the GCS supercomputer SuperMUC at Leibniz Supercomputing Centre. Some parts of computations were also performed on the computing resources granted by RWTH Aachen University and Lichtenberg High-Performance Computer in Darmstadt.

References

[1] J. Janicka, A. Sadiki, Large eddy simulation of turbulent combustion systems, Proc. Combust. Inst. 30 (1) (2005) 537–547.
[2] H. Pitsch, Large-eddy simulation of turbulent combustion, Annu. Rev. Fluid Mech. 38 (1) (2006) 453–482.
[3] W. Moroń, W. Rybak, Ignition behaviour and flame stability of different ranks coals in oxy fuel atmosphere, Fuel 161 (2015) 174–181.
[4] T.H. Fletcher, Review of 30 years of research using the chemical percolation devolatilization model, Energy Fuels 33 (12) (2019) 12123–12153.
[5] S. Badzioch, P.G. Hawksley, Kinetics of thermal decomposition of pulverized coal particles, Ind. Eng. Chem. Process Des. Dev. 9 (4) (1970) 521–530.
[6] H. Kobayashi, J. Howard, A.F. Sarofim, Coal devolatilization at high temperatures, Symposium (International) on Combustion, 16, Elsevier (1977), pp. 411–425.
[7] M. Vascellari, R. Arora, M. Pollack, C. Hasse, Simulation of entrained flow gasification with advanced coal conversion submodels. part 1: pyrolysis, Fuel 113 (2013) 654–669.
[8] M. Vascellari, H. Xu, C. Hasse, Flamelet modeling of coal particle ignition, Proc. Combust. Inst. 34 (2) (2013) 2445–2452.
[9] J. Watanabe, K. Yamamoto, Flamelet model for pulverized coal combustion, Proc. Combust. Inst. 35 (2) (2015) 2315–2322.
[10] R. Knappstein, G. Kuenne, T. Meier, A. Sadiki, J. Janicka, Evaluation of coal particle volatiles reaction by using detailed kinetics and FGM tabulated chemistry, Fuel 201 (2017) 39–52.
[11] H. Nicolai, T. Li, C. Geschwindner, F. di Mare, C. Hasse, B. Boehm, J. Janicka, Numerical investigation of pulverized coal particle group combustion using tabulated chemistry, Proc. Combust. Inst. (2020).
[12] M. Rieth, A. Clements, M. Rabaçal, F. Proch, O. Stein, A. Kempf, Flamelet les modeling of coal combustion with detailed devolatilization by directly coupled cpd, Proc. Combust. Inst. 36 (2) (2017) 2181–2189.
[13] E. Knudsen, H. Pitsch, A general flamelet transformation useful for distinguishing between premixed and non-premixed modes of combustion, Combust. Flame 156 (3) (2009) 678–696.
[14] E. Knudsen, H. Pitsch, et al., Modeling partially premixed combustion behavior in multiphase les, Combust. Flame 162 (1) (2015) 159–180.
[15] K. Luo, H. Pitsch, M. Pai, O. Desjardins, Direct numerical simulations and analysis of three-dimensional n-heptane spray flames in a model swirl combustor, Proc. Combust. Inst. 33 (2) (2011) 2143–2152.
[16] X. Wen, M. Rieth, A. Scholtissek, O.T. Stein, H. Wang, K. Luo, A.M. Kempf, A. Kronenburg, J. Fan, C. Hasse, A comprehensive study of flamelet tabulation methods for pulverized coal combustion in a turbulent mixing layer-part i: a priori and budget analyses, Combust. Flame 216 (2020) 439–452.
[17] C.R. Shaddix, A. Molina, Particle imaging of ignition and devolatilization of pulverized coal during oxy-fuel combustion, Proc. Combust. Inst. 32 (2) (2009) 2091–2098.
[18] A. Molina, C.R. Shaddix, Ignition and devolatilization of pulverized bituminous coal particles during oxygen/carbon dioxide coal combustion, Proc. Combust. Inst. 31 (2) (2007) 1905–1912.
[19] J. Köser, L.G. Becker, A.-K. Goßmann, B. Böhm, A. Dreizler, Investigation of ignition and volatile combustion of single coal particles within oxygen-enriched atmospheres using high-speed oh-plif, Proc. Combust. Inst. 36 (2) (2017) 2103–2111.
[20] J. Köser, T. Li, N. Vorobiev, A. Dreizler, M. Schiemann, B. Böhm, Multi-parameter diagnostics for high-resolution in-situ measurements of single coal particle combustion, Proc. Combust. Inst. 37 (3) (2019) 2893–2900.
[21] S. Farazi, A. Attili, S. Kang, H. Pitsch, Numerical study of coal particle ignition in air and oxy-atmosphere, Proc. Combust. Inst. 37 (3) (2019) 2867–2874.
[22] B. Goshayeshi, J.C. Sutherland, A comparison of various models in predicting ignition delay in single-particle coal combustion, Combust. Flame 161 (7) (2014) 1900–1910.
[23] S. Jimenez, C. Gonzalo-Tirado, Properties and relevance of the volatile flame of an isolated coal particle in conventional and oxy-fuel combustion conditions, Combust. Flame 176 (2017) 94–103.
[24] G.P. Smith,et al. Gri 3.0, 2019, accessed, June.
[25] R. Knappstein, G. Kuenne, A. Ketelheun, J. Köser, L. Becker, S. Heuer, M. Schiemann, V. Scherer, A. Dreizler, A. Sadiki, et al., Devolatilization and volatiles reaction of individual coal particles in the context of FGM tabulated chemistry, Combust. Flame 169 (2016) 72–84.
[26] A. Attili, P. Farmand, C. Schumann, S. Farazi, B. Böhm, T. Li, C. Geschwindner, J. Köser, A. Dreizler, H. Pitsch, Numerical simulations and experiments of ignition of solid particles in a laminar burner: effects of slip velocity and particle swelling, Flow Turbul. Combust. (2020) 1–17.
[27] Y. Liu, M. Geier, A. Molina, C.R. Shaddix, Pulverized coal stream ignition delay under conventional and oxy-fuel combustion conditions, Int. J. Greenh. Gas Control 5 (2011) S36–S46.
[28] T. Li, C. Geschwindner, J. Köser, M. Schiemann, A. Dreizler, B. Böhm, Investigation of the transition from single to group coal particle combustion using high-speed scanning oh-lif and diffuse backlight-illumination, Proc. Combust. Inst. 20 (6) (2020) 487, doi:10.1016/j.proci.2020.06.314.
[29] S. Farazi, J. Hinrichs, M. Davidovic, T. Falkenstein, M. Bode, S. Kang, A. Attili, H. Pitsch, Numerical investigation of coal particle stream ignition in oxy-atmosphere, Fuel 241 (2019) 477–487.
[30] G. Tufano, O. Stein, B. Wang, A. Kronenburg, M. Rieth, A. Kempf, Coal particle volatile combustion and flame interaction. Part I: characterization of transient and group effects, Fuel 229 (2018) 262–269.
[31] T. Sayadi, S. Farazi, S. Kang, H. Pitsch, Transient multiple particle simulations of char particle combustion, Fuel 199 (2017) 289–298.
[32] R.H. Essenhigh, M.K. Misra, D.W. Shaw, Ignition of coal particles: a review, Combust. Flame 77 (1) (1989) 3–30.
[33] K. Annamalai, P. Durbetaki, A theory on transition of ignition phase of coal particles, Combust. Flame 29 (1977) 193–208.
[34] Y. Yuan, S. Li, G. Li, N. Wu, Q. Yao, The transition of heterogeneous–homogeneous ignitions of dispersed coal particle streams, Combust. Flame 161 (9) (2014) 2458–2468.
[35] P.A. Bejarano, Y.A. Levendis, Single-coal-particle combustion in o2/n2 and o2/co2 environments, Combust. Flame 153 (1–2) (2008) 270–287, doi:10.1016/j.combustflame.2007.10.022.
[36] Y.A. Levendis, K. Joshi, R. Khatami, A.F. Sarofim, Combustion behavior in air of single particles from three different coal ranks and from sugarcane bagasse, Combust. Flame 158 (3) (2011) 452–465, doi:10.1016/j.combustflame.2010.09.007.
[37] J. Riaza, R. Khatami, Y.A. Levendis, L. Álvarez, M.V. Gil, C. Pevida, F. Rubiera, J.J. Pis, Single particle ignition and combustion of anthracite, semi-anthracite and bituminous coals in air and simulated oxy-fuel conditions, Combust. Flame 161 (4) (2014) 1096–1108, doi:10.1016/j.combustflame.2013.10.004.
[38] O. Desjardins, G. Blanquart, G. Balarac, H. Pitsch, High order conservative finite difference scheme for variable density low mach number turbulent flows, J. Comput. Phys. 227 (15) (2008) 7125–7159.
[39] A. Attili, F. Bisetti, M.E. Mueller, H. Pitsch, Formation, growth, and transport of soot in a three-dimensional turbulent non-premixed jet flame, Combust. Flame 161 (7) (2014) 1849–1865, doi:10.1016/j.combustflame.2014.01.008.
[40] L. Berger, K. Kleinheinz, A. Attili, H. Pitsch, Characteristic patterns of thermodiffusively unstable premixed lean hydrogen flames, Proc. Combust. Inst. 37 (2) (2019) 1879–1886.
[41] R.D. Falgout, U.M. Yang, hypre: a library of high performance preconditioners, in: P.M.A. Sloot, A.G. Hoekstra, C.J.K. Tan, J.J. Dongarra (Eds.), Computational Science — ICCS 2002, Springer, Berlin, Heidelberg (2002), pp. 632–641.
[42] S. Farazi, M. Sadr, S. Kang, M. Schiemann, N. Vorobiev, V. Scherer, H. Pitsch, Resolved simulations of single char particle combustion in a laminar flow field, Fuel 201 (2017) 15–28.
[43] T. Lehnhäuser, M. Schäfer, Improved linear interpolation practice for finite-volume schemes on complex grids, Int. J. Numer. Methods Fluids 38 (2002) 625–645.
[44] G. Zhou, L. Davidson, E. Olsson, Transonic inviscid/turbulent airfoil flow simulations using a pressure based method with high order schemes(1995) 372–378.
[45] H.L. Stone, Iterative solution of implicit approximations of multidimensional partial differential equations, SIAM J. Numer. Anal. 5(3) (1968) 530–558.
[46] G.L. Tufano, O.T. Stein, A. Kronenburg, A. Frassoldati, T. Faravelli, L. Deng, A.M. Kempf, M. Vascellari, C. Hasse, Resolved flow simulation of pulverized coal particle devolatilization and ignition in air- and O_2/CO_2-atmospheres, Fuel 186 (2016) 285–292.
[47] M. Baum, P. Street, Predicting the combustion behaviour of coal particles, Combust. Sci. Technol. 3 (5) (1971) 231–243.
[48] R. Knappstein, G. Kuenne, H. Nicolai, F. di Mare, A. Sadiki, J. Janicka, Description of the char conversion process in coal combustion based on premixed FGM chemistry, Fuel 236 (2019) 124–134.
[49] D.M. Grant, R.J. Pugmire, T.H. Fletcher, A.R. Kerstein, Chemical model of coal devolatilization using percolation lattice statistics, Energy Fuels 3 (2) (1989) 175–186.
[50] S. Umemoto, S. Kajitani, K. Miura, H. Watanabe, M. Kawase, Extension of the chemical percolation devolatilization model for predicting formation of tar compounds as soot precursor in coal gasification, Fuel Process. Technol. 159 (2017) 256–265.
[51] T.H. Fletcher, A.R. Kerstein, R.J. Pugmire, D.M. Grant, Chemical percolation model for devolatilization. 2. temperature and heating rate effects on product yields, Energy Fuels 4 (1) (1990) 54–60.
[52] W. Ranz, W.R. Marshall, et al., Evaporation from drops, Chem. Eng. Prog. 48 (3) (1952) 141–146.
[53] D. Merrick, Mathematical models of the thermal decomposition of coal: 2. Specific heats and heats of reaction, Fuel 62 (5) (1983) 540–546.
[54] B.S. Brewster, L.L. Baxter, L.D. Smoot, Treatment of coal devolatilization in comprehensive combustion modeling, Energy Fuels 2 (4) (1988) 362–370.
[55] A. Attili, F. Bisetti, M.E. Mueller, H. Pitsch, Effects of non-unity lewis number of gas-phase species in turbulent nonpremixed sooting flames, Combust. Flame 166 (2016) 192–202.

[56] L. Cai, S. Kruse, D. Felsmann, H. Pitsch, A methane mechanism for oxy-fuel combustion: extinction experiments, model validation, and kinetic analysis, Flow Turbul. Combust. (2020).
[57] J. Van Oijen, A. Donini, R. Bastiaans, J. ten Thije Boonkkamp, L. De Goey, State-of-the-art in premixed combustion modeling using flamelet generated manifolds, Prog. Energy Combust. Sci. 57 (2016) 30–74.
[58] Chem1D, A one-dimensional laminar flame code, developed at Eindhoven university of technology, 2018accessed, May.
[59] L.D. Timothy, A.F. Sarofim, J.M. Béer, Characteristics of single particle coal combustion, Symp. (Int.) Combust. 19 (1) (1982) 1123–1130, doi:10.1016/S0082-0784(82)80288-9.
[60] R. Khatami, Y.A. Levendis, An overview of coal rank influence on ignition and combustion phenomena at the particle level, Combust. Flame 164 (2016) 22–34, doi:10.1016/j.combustflame.2015.10.031.
[61] T. Li, M. Schiemann, J. Köser, A. Dreizler, B. Böhm, Experimental investigations of single particle and particle group combustion in a laminar flow reactor using simultaneous volumetric oh-lif imaging and diffuse backlight-illumination, Renew. Sustain. Energy Rev. 136 (2021) 110377, doi:10.1016/j.rser.2020.110377.
[62] T. Li, P. Farmand, C. Geschwindner, M. Greifenstein, J. Köser, C. Schumann, A. Attili, H. Pitsch, A. Dreizler, B. Böhm, Homogeneous ignition and volatile combustion of single solid fuel particles in air and oxy-fuel conditions, Fuel 291 (1) (2021) 120101, doi:10.1016/j.fuel.2020.120101.
[63] T. Li, B. Zhou, J.H. Frank, A. Dreizler, B. Böhm, High-speed volumetric imaging of formaldehyde in a lifted turbulent jet flame using an acousto-optic deflector, Exp. Fluids 61 (4) (2020) 2903.
[64] H. Nicolai, G. Kuenne, R. Knappstein, H. Schneider, L. Becker, C. Hasse, F. di Mare, A. Dreizler, J. Janicka, Large eddy simulation of a laboratory-scale gas-assisted pulverized coal combustion chamber under oxy-fuel atmospheres using tabulated chemistry, Fuel 272 (2020) 117683.
[65] H. Nicolai, X. Wen, F. Miranda, D. Zabrodiec, A. Massmeyer, F. di Mare, A. Dreizler, C. Hasse, R. Kneer, J. Janicka, Numerical investigation of swirl-stabilized pulverized coal flames in air and oxy-fuel atmospheres by means of large eddy simulation coupled with tabulated chemistry, Fuel 287 (2020) 119429.
[66] M. Rabaçal, M. Costa, M. Rieth, A.M. Kempf, Particle history from massively parallel large eddy simulations of pulverised coal combustion in a large-scale laboratory furnace, Fuel 271 (2020) 117587.